Commun Nonlinear Sci Numer Simulat 91 (2020) 105416

Contents lists available at ScienceDirect

Commun Nonlinear Sci Numer Simulat

journal homepage: www.elsevier.com/locate/cnsns

Research paper

Stability transition of persistence and extinction in an avian influenza model with Allee effect and stochasticity

Yu Liu[a,b], Shigui Ruan[c], Ling Yang[a,b,*]

[a] School of Mathematical Sciences, Soochow University, Suzhou 215006, P. R. China
[b] Center for Systems Biology, Soochow University, Suzhou 215006, P. R. China
[c] Department of Mathematics, University of Miami, Coral Gables, FL 33146, United States

ARTICLE INFO

Article history:
Received 23 January 2020
Revised 16 June 2020
Accepted 17 June 2020
Available online 24 June 2020

Keywords:
Stability transition
Population persistence and extinction
FPK equation
Noise

ABSTRACT

Population persistence and extinction are the most important issues in ecosystems. In the past a few decades, various deterministic and stochastic mathematical models with Allee effect have been extensively studied. However, in both population and disease dynamics, the question of how structural transitions caused by internal or external environmental noise emerge has not been fully elucidated. In this paper, we introduce a semi-analytical method to explore the asymptotically convergent behavior of a stochastic avian influenza model with Allee effect. First, by introducing noise to the model, we observe numerically a significant transition from bistability to monostability. Next, a corresponding Fokker-Planck (FPK) equation is obtained to analytically describe the probability density distributions with long time evolution in order to reveal the transition characteristics. Ratio of the approximately convergent probabilities for the two key equilibria derived from the FPK equation confirms the stability transition observed by previous numerical simulations. Moreover, bifurcation analysis in two important parameters demonstrates that noise not only reduces the parametric zone of sustaining bistability but also drives the system to exhibit different monostabilities, which correspond numerically to population persistence and extinction at different parametric intervals, respectively. Furthermore, noise induces higher probabilities for the system to sustain persistence instead of extinction in this model. Our results could provide some suggestions to improve wildlife species survival in more realistic situations where noise exists.

1. Introduction

Since ecological balance is becoming more and more important in the development of living beings, determining the persistence-extinction threshold of different populations has been one of the dominant topics in modeling population dynamics and infectious diseases. Persistence-extinction transition occurs in investigating many biological and ecological processes, such as disease outbreaks, species competition and predation [1], resource management, and so on [2]. Influenza A viruses are well known as fatal agents to cause infections in wildlife including birds, which can also be transmitted between humans and birds directly as well as indirectly. Various mathematical models have been developed to analyze the

* Corresponding author.
E-mail address: lyang@suda.edu.cn (L. Yang).

https://doi.org/10.1016/j.cnsns.2020.105416
1007-5704/

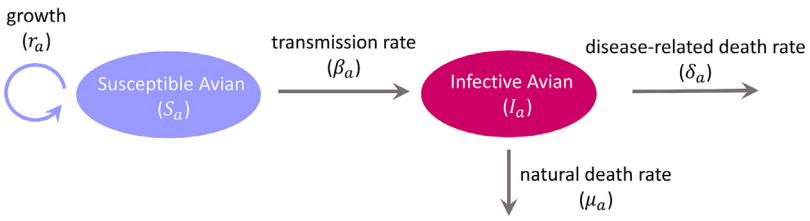

Fig. 1. The flowchart of the SI avian influenza epidemic model.

epidemiological characteristics of avian influenza and to provide efficient control measures in order to reduce mortality [3, 4].

As one of the main sources for transmitting diseases to humans, avian populations are often assumed to experience a natural phenomenon called Allee effect [5]. Due to the strength and prevalence of Allee effect in natural animal populations [6-10], many population models with the Allee effect have been proposed and analyzed. Hilker et al. [11] constructed models with a strong Allee effect and observed rich dynamics including the existence of homoclinic loops with eventual host extinction. Friedman et al. [12] considered an epidemic model for a fatal disease in a population with Allee effect and obtained conditions leading to host persistence or extinction.

However, population dynamics are always coupled with various types of environmental noise in the real world. The environment factors vary randomly and could be stochastic [13]. In fact, stochastic population systems driven by Brownian motion have been employed to address the transition of persistence-extinction [14-18]. Ghanbari et al. [19] studied an avian-human influenza model perturbed by environmental white noise. Zhang et al. [20] discussed the dynamics of a stochastic avian-human influenza epidemic model with mutation. Krstic and Jovanovic [21] focused on a one-dimensional stochastic differential equation (SDE) model with the Allee effect and explored the existence, uniqueness and asymptotic stability of solutions, including situations where populations went extinct. Jovanović and Krstic [22] also gave sufficient conditions for the population extinction by using a one-dimensional stochastic time-dependent delay population model with the Allee effect. Recently, Bashkirtseva [23] focused on a phenomenological Hassell mathematical model with Allee effect and found that the persistence zone can decrease and even disappear under random noise. Those results demonstrated that noise could lead to population extinction. Hence, whether noise induces species persistence or extinction and how an underlying structural transition occurs deserves to be elucidated systemically. Fig. 1.

Based on the above discussions, we attempt to introduce stochastic perturbations into an avian influenza model with Allee effect and investigate how random disturbances affect dynamic behaviors of the model. The paper is organized as follows. In Section 2, an avian influenza epidemic model with Allee effect but without noise and its dynamics are presented. In Section 3, we show preliminarily that noise leads to a stability transition from bistability to monostability and explain the results by using the corresponding Fokker-Planck (FPK) equation. In Sections 4–6, noise-induced transitions from the perspective of two key parameters are studied, respectively. The results indicate that under increasing noise, the system seems to be monostable rather than bistable. Moreover, the parametric zone where the population stays only persistent in the disturbed system becomes larger compared with the undisturbed one.

2. The avian influenza model with Allee effect and without noise perturbation

To study the influence of noise perturbations on the dynamic behaviors, we first consider a well-defined avian influenza model with Allee effect from Liu et al. [24] as a basic description of a bird population infected by influenza A virus. In the two-dimensional model, the avian population is divided into two groups: susceptible and infective at time t, denoted by $S_a(t)$ and $I_a(t)$, respectively. Besides, the following assumptions have been made:

(1) Susceptible avian population is subjected to logistic growth and Allee effect;
(2) An infected avian keeps in the state of disease and cannot recover;
(3) The incidence rate between the susceptible avian and the infective avian is bilinear.

Based on the above assumptions, we have the following SI avian influenza model (denoted as Model A):

$$\begin{aligned}\frac{dS_a}{dt} &= r_a S_a\left(1-\frac{S_a}{M_a}\right)\left(\frac{S_a}{m_a}-1\right)-\beta_a S_a I_a = F_1(S_a, I_a)\\ \frac{dI_a}{dt} &= \beta_a S_a I_a-(\mu_a+\delta_a)I_a = F_2(S_a, I_a)\end{aligned} \tag{1}$$

where r_a is the intrinsic growth rate, M_a is the maximal carrying capacity, m_a is the critical carrying capacity of the avian population, β_a is the transmission rate from infective avian to susceptible avian, μ_a is the natural death rate of the avian population, δ_a is the disease-related death rate of the infected avian.

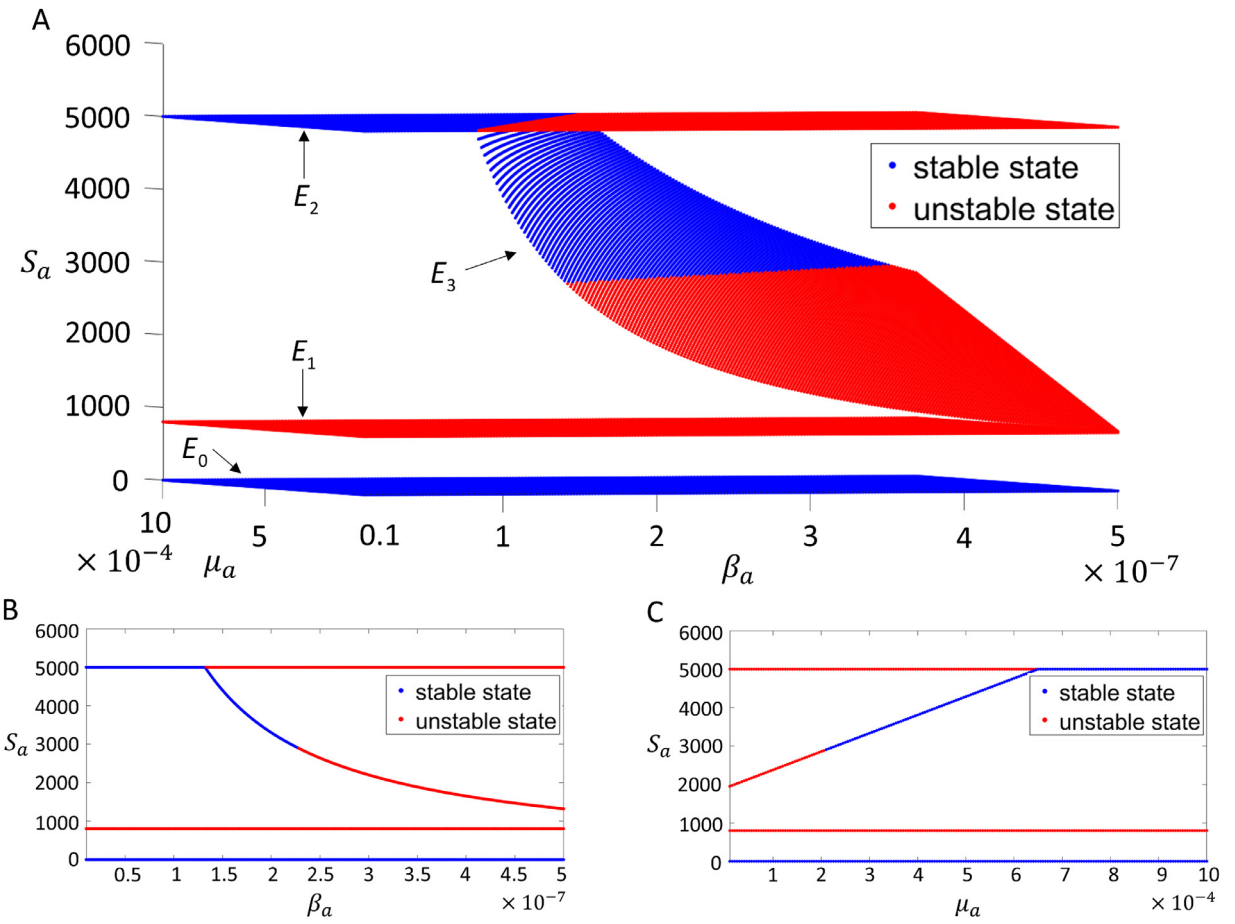

Fig. 2. The bifurcation diagram of S_a versus two key parameters. Parameters are set by $\delta_a = 4 \times 10^{-4}$, $r_a = 5 \times 10^{-3}$, $M_a = 5000$, $m_a = 800$. (*A*) β_a varies from 1×10^{-8} to 5×10^{-7} and μ_a varies from 1×10^{-5} to 1×10^{-3}; (*B*) $\mu_a = 2.6 \times 10^{-4}$; (*C*) $\beta_a = 2.1 \times 10^{-7}$.

Defining the basic reproduction number by

$$R = \frac{\beta_a (M_a + m_a)(\mu_a + \delta_a)}{(\mu_a + \delta_a)^2 + M_a m_a \beta_a^2}$$

Three disease-free equilibria of Model A can be deduced as $E_0 = (0, 0)$, $E_1 = (m_a, 0)$ and $E_2 = (M_a, 0)$. If $R > 1$, that is, $m_a < \frac{\mu_a + \delta_a}{\beta_a} < M_a$, a unique endemic equilibrium can also be given by $E_3 = (S^*, I^*)$, where

$$S^* = \frac{\mu_a + \delta_a}{\beta_a}, \quad I^* = \frac{r_a}{\beta_a} \frac{M_a m_a \beta_a^2 + (\mu_a + \delta_a)^2}{M_a m_a \beta_a^2} (R - 1)$$

The parameters δ_a, r_a, M_a and m_a are from [24]. The disease-induced death rate of the infected avian is $\delta_a = 4 \times 10^{-4}$ per day and the intrinsic growth rate of the avian population is $r_a = 5 \times 10^{-3}$ per day. Besides, the maximal and critical carrying capacities of the avian population are $M_a = 5000$ and $m_a = 800$, respectively. All parameters are selected based on the biological facts, for example, the natural death rate μ_a is set by assuming that the wild avian can survive about 8 years (see [24] for more details).

Considering the expression of E_3, we fix δ_a, r_a, M_a and m_a, and consider two key parameters β_a and μ_a. The bifurcation diagram of Model A depicting the steady state solution of S_a with respect to two parameters β_a and μ_a is shown in Fig. 2. In Fig. 2A, β_a and μ_a vary from 1×10^{-8} to 5×10^{-7} and 1×10^{-5} to 1×10^{-3}, respectively. Here, $E_0 = (0, 0)$ is always stable (blue dots) while $E_1 = (m_a, 0)$ is always unstable (red dots). Meanwhile, $E_2 = (M_a, 0)$ becomes unstable with a larger β_a or a smaller μ_a. Once parameters satisfy $m_a < \frac{\mu_a + \delta_a}{\beta_a} < M_a$ the endemic equilibrium $E_3 = (S^*, I^*)$ emerges (a corresponding sloping plane occurs). Previous study of [24] has already verified that if $\frac{m_a + M_a}{2} \leq \frac{\mu_a + \delta_a}{\beta_a} < M_a$, then E_3 is globally asymptotically stable. If $m_a < \frac{\mu_a + \delta_a}{\beta_a} < \frac{m_a + M_a}{2}$, then E_3 becomes unstable. Fig. 2A also shows that E_3 becomes unstable with a larger β_a or a smaller μ_a and only remains stable within a certain area. Specifically, Figs. 2B and 2C present the bifurcation diagram of S_a versus β_a or μ_a, with $\mu_a = 2.6 \times 10^{-4}$ and $\beta_a = 2.1 \times 10^{-7}$ respectively.

3. Preliminary analysis of the model with noise perturbations

Due to the existence of inevitable environmental fluctuations in the real world, noise is introduced into Model A in order to study the population dynamics. In this paper, we consider the effect of fluctuations by stochastically perturbing the rates of the two sub-populations along time. Consequently, for a population vector $X = (S_a, I_a)^T$, we have

$$\frac{dX}{dt} = F(x) \rightarrow \frac{dX}{dt} = F(x) + \zeta$$

where ζ is the noise force from the fluctuations and it can often be deemed to Gaussian and white noise: $\langle \zeta(t)\zeta(t')\rangle = 2D\delta(t-t')$. D is the diffusion coefficient tensor (matrix) measuring the level of noise strength. Then we obtain Model B as follows:

$$\begin{aligned} \frac{dS_a}{dt} &= r_a S_a\left(1-\frac{S_a}{M_a}\right)\left(\frac{S_a}{m_a}-1\right) - \beta_a S_a I_a + \zeta \\ \frac{dI_a}{dt} &= \beta_a S_a I_a - (\mu_a + \delta_a) I_a + \zeta \end{aligned} \tag{2}$$

In the following, parameters δ_a, r_a, M_a and m_a in Model B are set to be the same as in section 2. To explore whether noise changes the bistability of model A, we focus on the parametric zone where the two parameters β_a and μ_a satisfy the following condition:

$$\frac{m_a + M_a}{2} \leq \frac{\mu_a + \delta_a}{\beta_a} < M_a$$

under which model A is bistable with two stable steady states E_0 and E_3, respectively.

In order to explore the effects of noise on Model A, we compare the final convergence of both models under the same initial conditions. By assuming that the wild avian can survive about 8 years, the natural death rate is $\mu_a = 3.4246 \times 10^{-4}$ per day. The transmission rate is set to be $\beta_a = 2.44 \times 10^{-7}$. Here, we screen 100 pairs of initial values by even distribution with S_a between 0 and 4000 and I_a between 0 and 25,000, respectively. The numerical simulations of S_a with respect to time are given in Fig. 3. The Euler-Maruyama (EM) method [25] (see Supplemental A for detailed information) is adopted for analyzing the characteristics of Model B. Additionally, the non-positive values of S_a due to the stochastic noise is truncated and set to zero in aim to fit the realism. As we can see, Model A eventually converges to two equilibria, E_0 representing population extinction and E_3 represents population persistence (Fig. 3A). In fact, the stability region for the stable steady state E_3 is relatively larger than that for E_0, which implies that the probability of converging to E_3 is higher than to E_0. While considering Model B, we observe totally different phenomena (Fig. 3B-C). When noise is weak, the value S_a starts to fluctuate in a small region (Fig. 3B). By enhancing the intensity of noise, all values of S_a fall into the neighborhood of zero; namely, the preceding high populations fail to maintain (Fig. 3C). It is interesting to note that noise brings a change to stability of Model A, this explains the emergence of monostability (population extinction in this case) in the real world instead of bistability shown in the deterministic Model A.

Since noise can cause stability transition as shown in Fig. 3, we aim to explicitly elucidate the stability behaviors of Model B based on the two parameters, β_a and μ_a, and the noise intensity D.

To analyze the asymptotical stability of Model B, Fokker-Planck (FPK) equation is introduced to reveal the global principles [26]. Based on the stochastic differential equations (2), we can deduce the corresponding probability density distribution equation with noise due to fluctuations as follows:

$$\frac{\partial P(S_a, I_a, t)}{\partial t} = -\frac{\partial}{\partial S_a}[F_1(S_a, I_a)P] - \frac{\partial}{\partial I_a}[F_2(S_a, I_a)P] + D\left(\frac{\partial^2 P}{\partial S_a^2}\right) + D\left(\frac{\partial^2 P}{\partial I_a^2}\right)$$

where P represents the probability density distribution of Model B subjected to S_a and I_a at time t. D is the diffusion coefficient tensor or matrix, which is assumed to be homogeneous and isotropic constant for simplicity ($D_{11} = D_{22} = D$ and $D_{12} = D_{21} = 0$). F_1 and F_2 are shown in Model A (1).

Due to the difficulty of finding theoretical solutions for $P(S_a, I_a, t)$ and analytical solutions for its approximate equations when $t \rightarrow \infty$, we manage to solve $P(S_a, I_a, t)$ numerically by VCell software [27]. Because of the convergence to the first quadrant for Model A, we designate a calculational area for numerical simulations of the probability density distribution equation where the equilibria E_0 and E_3 are included, respectively. And we set the boundaries to be no-flow boundary conditions. Besides, initial value is given by $P(S_a, I_a, 0) = 1$ and the long time limit is taken in the numerical simulations so that the probability density distribution nearly makes no change (for example, $t = 300000$).

Fig. 4 illustrates that with various intensities of noise, the steady-state probability density distribution of Model B is completely different. Specifically, a transition from bistability to monostability emerges when the noise is enhanced.

At first, when $\beta_a = 2.44 \times 10^{-7}$ and the noise intensity is set low, the probability density distribution shows that most probability densities that mainly distribute around E_3 transfer finally to the area around E_0 (Fig. 4A). Further, when the noise becomes stronger, as shown in Fig. 4B, probabilities can hardly gather around E_3 and the system is approximately considered to be monostable. The same change can also be observed with $\beta_a = 2.48 \times 10^{-7}$ (Fig. 4C-D). As a result, when noise is relatively strong, Model B shows a change of the structure in probability density distribution from bistability to monostability.

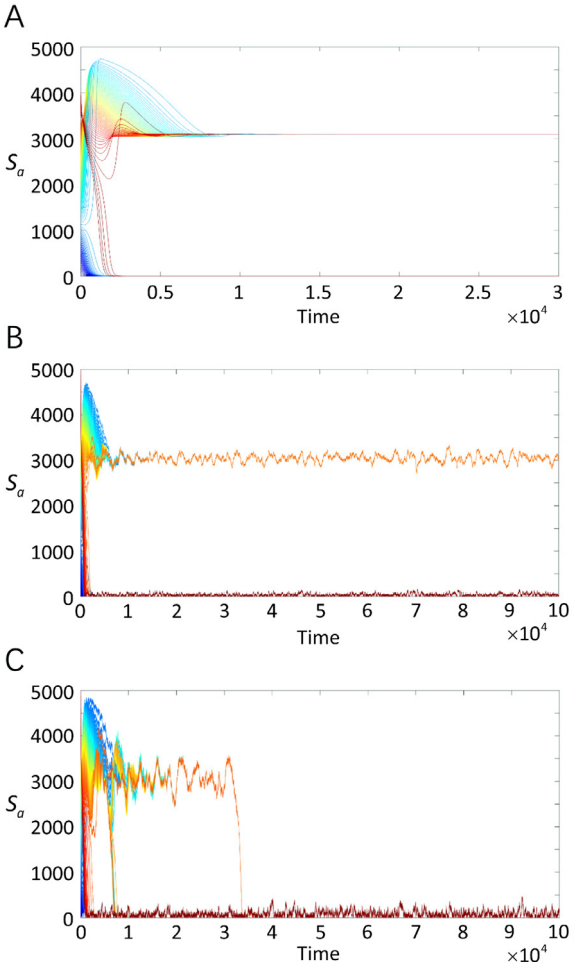

Fig. 3. The expression of S_a under different noise perturbations. $(A)D = 0$; $(B)D = 10$; $(C)D = 50$.

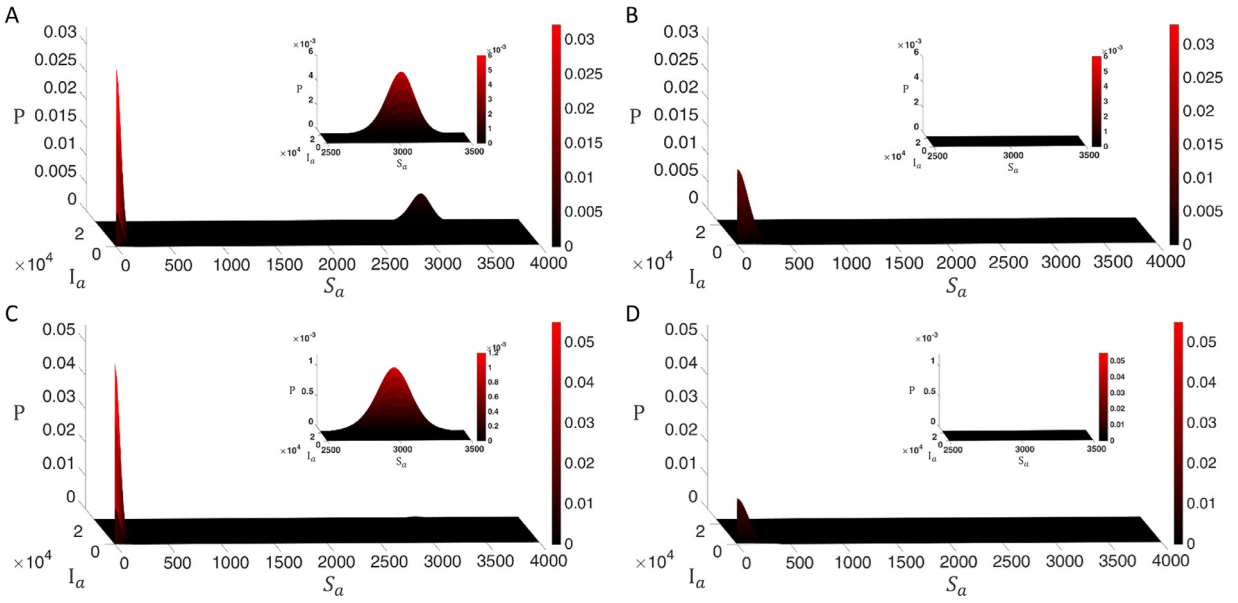

Fig. 4. Probability density distributions of Model B. $(A)\beta_a = 2.44 \times 10^{-7}, D = 10; (B)\beta_a = 2.44 \times 10^{-7}, D = 50$; $(C)\beta_a = 2.48 \times 10^{-7}, D = 10$; $(D)\beta_a = 2.48 \times 10^{-7}, D = 50$. The four insert graphs are the local enlarged distributions when $2500 \leq \beta_a \leq 3500$.

Table 1
The ratios of probability around E_0 and E_3 for different β_a and D values.

Parameter Condition	β_a	$D = 10$				$D = 50$			
		P_0	P_3	$P_0 + P_3$	RoP	P_0	P_3	$P_0 + P_3$	RoP
$\frac{m_a+M_a}{2} \le \frac{\mu_a+\delta_a}{\beta_a} < M_a$	2.44×10^{-7}	0.4981	0.4693	0.9674	1.061	0.9956	0.0003581	0.9960	2781
	2.48×10^{-7}	0.8377	0.1328	0.9705	6.308	0.9962	0.0001472	0.9963	6777

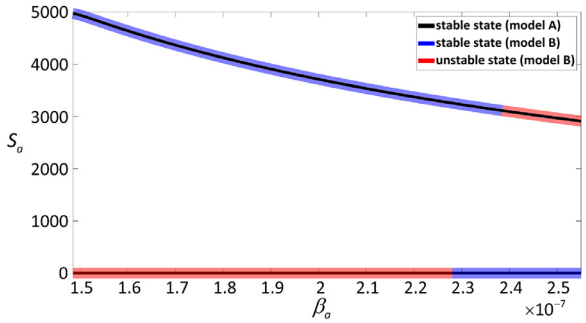

Fig. 5. Convergence of S_a when β_a varies in model A and model B.

Although Fig. 4 displays the stability transition of Model B from bistability to monostabilty primarily, it is noticeable that probability densities of two local regions, one containing E_0 and the other containing E_3, are both decreasing, and at the same time the corresponding non-zero area becomes larger. Thus, it is necessary to examine the dominant role of the steady state E_0 when the noise is strong enough. This leads to the comparison of probabilities around E_0 and E_3.

Here, we interpret two rectangular areas with length of 3000 and width of 1200 as R_0 and R_3 (probability densities in the rest area are almost zero), with the corresponding center at E_0 and E_3, respectively. The probability around E_0 or E_3 can be regarded as the integral of the probability density within R_0 or R_3, which is denoted, respectively, by

$$P_0 = \int_{(S_a,I_a)\in R_0} P(S_a, I_a) \; and \; P_3 = \int_{(S_a,I_a)\in R_3} P(S_a, I_a)$$

Thus, the ratio of probabilities (*RoP*) around E_0 to E_3 can be defined by

$$RoP = P_0/P_3$$

If *RoP* is small enough, then Model B is considered to only approximately converge to E_3. If *RoP* is large, then Model B is regarded as to only approximately converges to E_0. Otherwise, Model B has two stable steady states. In the following analysis, we sum up probability densities to replace the integral result within each area.

Table 1 shows that the *RoP* makes quite a difference with an increased noise intensity, which indicates that a system tends to show a completely different stability behavior. When $\beta_a = 2.44 \times 10^{-7}$, the *RoP* is 1.061 with a lower noise intensity, while it turns to 2781 with a higher noise intensity. Additionally, when $\beta_a = 2.48 \times 10^{-7}$, the *RoPs* for two noise intensities are 6.308 and 6777, respectively. This means that most of the probabilities finally transfer to E_0 under stronger noise, which implies that Model B tends to extinction in this case. Hence, a smaller transmission rate β_a or noise intensity D helps Model B to avoid extinction in this case.

4. Stability transition of model B on the transmission rate β_a

In Section 3, it was observed that the noise has changed the final convergence of Model B. More specifically, an increased noise could lead to stability transition from bistability to monostability for both cases ($\beta_a = 2.44 \times 10^{-7}$ or $\beta_a = 2.48 \times 10^{-7}$). Given that β_a (the transmission rate from infective avian to susceptible avian) is a key parameter in Model B, it becomes quite necessary to study the impact of noise based on β_a.

Fig. 5 explains the convergence of Model A and Model B for different β_a values when parameter $\mu_a = 3.4246 \times 10^{-4}$ and noise intensity $D = 50$. Parameter β_a is chosen from 1.485×10^{-7} to 2.55×10^{-7}. Here, we exclude two steady states, E_1 and E_2, and focus on the other two, E_0 and E_3, which are both stable in Model A (thinner black lines). In the disturbed Model B, we assume that $RoP < 1$, Model B can finally be approximated to converge only to E_3. While if $RoP > 100$, Model B can be approximated to converge only to E_0. Otherwise, the system is considered to maintain bistable. It is noticeable that the stability of Model B within both ends (thicker translucent blue or red line) finally changes from bistability to monostability. When $1.485 \times 10^{-7} \le \beta_a \le 2.28 \times 10^{-7}$, E_0 becomes unstable and Model B converges only to E_3. Oppositely, when $2.385 \times 10^{-7} \le \beta_a \le 2.55 \times 10^{-7}$, E_3 becomes unstable and Model B converges only to E_0. A detailed stability transition process is given in Supplemental B (Figure S1) with six distinct β_a, respectively. The result shows that the noise motivates

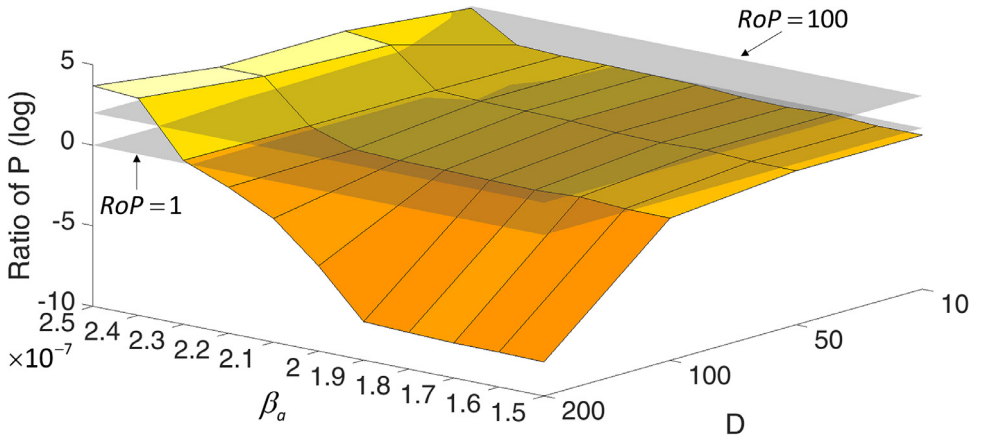

Fig. 6. The dependence of ratio of probabilities by the transmission rate β_a and noise intensity D.

the system to transfer from bistability to monostability, which means a transition from a coexistence of preservation and extinction to only preservation or extinction. Therefore, Fig. 5 provides a general vision on the effects that the noise brings to the system. With the presence of noise, stability of Model A could have totally changed and the system tends to be monostable instead of being bistable. Despite that, Model B could still sustain bistable within quite a small region compared with that in Model A. In addition, compared with Model A, the existence of noise in Model B is beneficial for the system to maintain preservation, because the parametric zone for Model B only converging to E_3 has been expanded a lot, which means a population is more resistant to noise disturbances.

We further delineate Fig. 6 to have a full look on the gradual changes by both the noise intensity D and the transmission rate β_a. On one hand, noise as a major element of the real world plays a significant role in population persistence and extinction. Model A converges to two stable steady states E_0 and E_3, respectively, when $\frac{m_a+M_a}{2} \leq \frac{\mu_a+\delta_a}{\beta_a} < M_a$. While in Model B, *RoP* is introduced to define the convergent situation. Due to the variance of *RoP*, the gradient yellow surface indicating $\log(RoP)$ by parameter β_a and noise intensity D is given in Fig. 6. The top and bottom horizontal translucent gray planes represent $\log(RoP) = 2$ ($RoP = 100$, denoted by plane 1) and $\log(RoP) = 0$ ($RoP = 1$, denoted by plane 2), respectively. Given the assumptions we have made, the area of the surface between two planes suggests that Model B maintains bistable. Moreover, the area above plane 1 or below plane 2 corresponds to the monostability of Model B, with one approximately converges to E_0 and the other to E_3 respectively. The increases of noise intensity D and β_a lead to the gradual increase of *RoP* above plane 1. While an increased D and a decreased β_a cause the sharp reduction of *RoP* under plane 2. It implies that Model B prefers monostability than bistability with noise perturbations. Moreover, when $D > 50$, the area of bistability show almost no change, which means that any additional noise could hardly shrink the bistable area.

On the other hand, the transmission rate β_a also contributes to the stability transition. When the transmission rate β_a in Model B increases, the increase of *RoP* can be observed, which indicates that the stable steady state of Model B changes from E_3 to E_0. This could cause population exacerbation and even extinction, as *RoP* turns pretty high. Moreover, when the noise intensity $D > 50$, the system prefers a monostable E_3 for the majority of parameter β_a ($1.5 \times 10^{-7} < \beta_a < 2.3 \times 10^{-7}$), which implies that noise intends to help the system to avoid extinction from the perspective of parameter β_a.

Therefore, different noise intensity D and transmission rate β_a could lead to various convergent situations for Model B, which can be inspiring for population persistence.

5. Stability transition of model B on the natural death rate μ_a

In section 4, we explained that monostability of the stochastically endemic equilibrium E_3 exists under certain range of noise intensity D. Besides, a smaller β_a also tends to help persistence. The big difference of stability behavior of Model B compared with Model A justifies the importance of parameter β_a. This leads to our exploration of another parameter μ_a to fully understand the dynamics of Model B.

For the analysis of parameter μ_a, which relates to the death rate of the infected avian, we set parameters by $\beta_a = 2 \times 10^{-7}$, $D = 50$ and let μ_a vary from 1.9×10^{-4} to 6×10^{-4}. As shown in Fig. 7, Model A still has two stable steady states E_0 and E_3 (thinner black lines), while the other two steady states E_1 and E_2 are unstable (not shown). Here, we assume that $RoP < 0.13$, Model B only approximately converges to E_3, while when $RoP > 1.37$, Model B only approximately converges to E_0. Otherwise, Model B is considered to be bistable. It is also noteworthy that the stability of Model B within both ends (thicker translucent blue or red line) finally changes from bistability to monostability, which is similar to what is shown in Fig. 5. When μ_a is relatively small ($1.9 \times 10^{-4} \leq \mu_a \leq 2.5 \times 10^{-4}$), E_3 becomes unstable and Model B converges to E_0. Oppositely, when μ_a is getting larger ($3.3 \times 10^{-4} \leq \mu_a \leq 6 \times 10^{-4}$), E_0 becomes unstable and Model B converges only to E_3. A detailed stability transition process is also given in Supplemental C (Figure S2) with six distinct μ_a, respectively. It is also

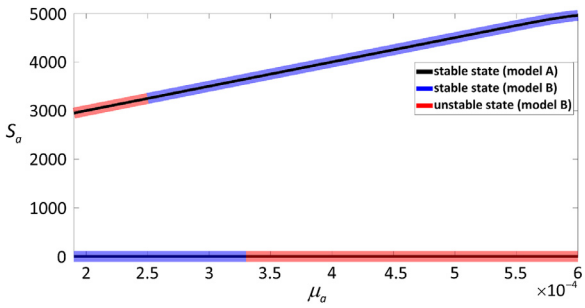

Fig. 7. Convergence of S_a when μ_a varies in model A and model B.

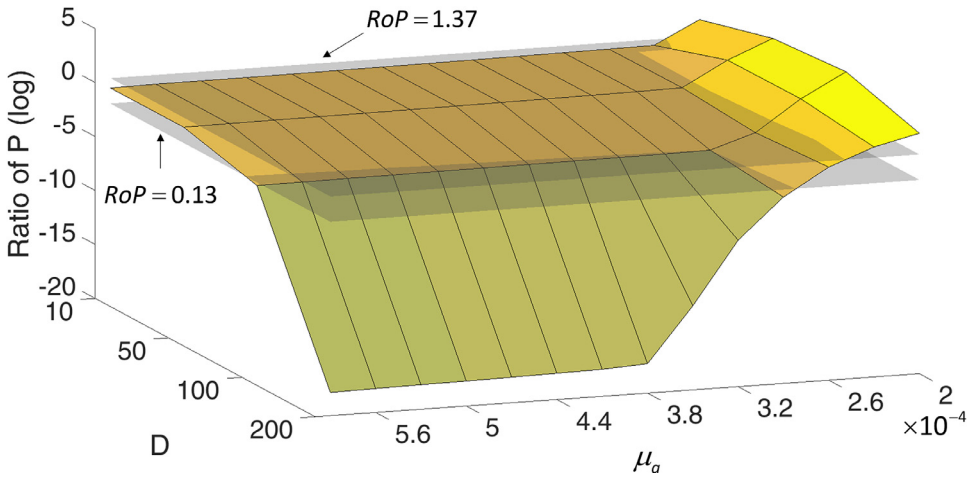

Fig. 8. The dependence of the ratio of probabilities on the death rate μ_a and noise intensity D.

worth noting that bistability still exists in a relatively smaller parametric zone ($2.5 \times 10^{-4} < \mu_a < 3.3 \times 10^{-4}$). Fig. 7 implies that noise totally changes the stability behavior of Model B, which leads to monostability of the system. Further, Model B is still bistable within a smaller region compared with Model A. Besides, the existence of noise is beneficial for a system to maintain only preservation compared to an undisturbed system. Namely, a system can survive under noise within a wider parametric zone of μ_a, which is consistent with the results obtained by analyzing β_a shown in Section 4.

Fig. 8 presents a gradient yellow surface of $\log(RoP)$ with respect to the noise intensity D and the natural death rate μ_a. The top and bottom horizontal translucent gray planes stand for $\log(RoP) = \log(1.37)$ ($RoP = 1.37$, denoted by plane 3) and $\log(RoP) = \log(0.13)$ ($RoP = 0.13$, denoted by plane 4), respectively. The area of the surface between two planes suggests that Model B approximately remains bistable. Moreover, the areas above plane 3 and below plane 4 correspond to monostability of Model B, while one is approximately convergent to E_0 and the other to E_3, respectively. Fig. 8 shows that noise contributes to the monostability of Model B. The increase of noise intensity D leads to the decrease of RoP below plane 4 while the area above plane 3 changes weakly. It indicates that the system may have higher probabilities to sustain around E_3 below plane 4, while it intends to maintain the original monostability above plane 3. Hence, the region above plane 3 or below plane 4 both explains that Model B prefers monostability than bistability with noise perturbations. Moreover, the bistability area changes significantly when D is around 100, from a larger parametric zone of μ_a when $D < 100$ ($2.4 \times 10^{-4} \le \mu_a \le 5.6 \times 10^{-4}$) to a narrowed one when $D > 100$ ($2.4 \times 10^{-4} \le \mu_a \le 2.8 \times 10^{-4}$).

Compared with β_a, it is interesting to notice that μ_a is less sensitive to the noise when $D < 100$. Besides, when $D > 100$, the RoP below plane 4 shows a great reduction when noise becomes stronger. Moreover, when increasing the natural rate μ_a, we observe a decrease of RoP, which indicates that the system tends to be stochastically asymptotically stable around E_3. It suggests that the system is tending to population persistence as the RoP turns pretty low. In addition, when $D > 100$, the system prefers monostability of E_3 for the majority of μ_a ($2.4 \times 10^{-4} \le \mu_a \le 5.6 \times 10^{-4}$), which implies that noise helps the system to maintain persistence. Therefore, a stronger noise D or a properly larger natural death rate μ_a may provide a certain system with persistence, which could offer some underlying suggestions for species protection.

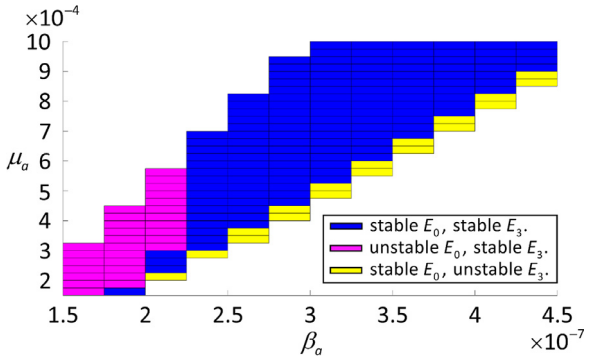

Fig. 9. Stability behaviors of model B under random noise by varying parameter β_a from 1.5×10^{-7} to 4.5×10^{-7} and μ_a from 1.5×10^{-4} to 1×10^{-3}, $D = 50$. The white area means that the condition $\frac{m_a+M_a}{2} \leq \frac{\mu_a+\delta_a}{\beta_a} < M_a$ (model A has two stable steady states E_0 and E_3) is not satisfied.

6. Stability transition of model B on both β_a and μ_a

In Sections 4 and 5, the stability transition of Model B was analyzed based on a specific parameter β_a or μ_a. In order to understand how stability transition may depend on both β_a and μ_a, Fig. 9 is further presented. Here, we focus on the parametric zone where Model A has two stable steady states E_0 and E_3. The assumptions are made as follows: If $RoP < 1$, then model B only approximately converges to E_3; If $RoP > 100$, then Model B only approximately converges to E_0. Otherwise, model B maintains bistable.

In Fig. 9, Model B exhibits three different stabilities when noise intensity is set as $D = 50$. E_0 becomes stable with an increased β_a or a decreased μ_a, while E_3 tends to be stable with a decreased β_a or an increased μ_a. The result also matches the stability transition analysis of β_a and μ_a, shown in Fig. 5 and Fig. 7, respectively, which emphasizes that noise induces monostability in Model B. Besides, Model B tends to be bistable in the upper right area. Since the wild avian can survive about 8 years, the corresponding natural death rate should be around $\mu_a = 3.4246 \times 10^{-4}$ per day, which indicates that the lower left parametric zone in Fig. 9 is closer to a real biological system. Hence, a disturbance to the system with relatively small β_a or μ_a can cause stability transition of Model B, from bistability to monostability, and the area where only E_3 being stable is larger than that with only E_0, which demonstrates a beneficial effect of noise for Model B to be persistent.

7. Discussion

In this paper, the dynamical transition in an avian epidemic model with Allee effect by stochastic perturbation has been extensively investigated. Numerical simulations were carried out and a crucial change of the system from bistability to monostability under noise has been observed. We further confirmed the convergent results by introducing an FPK equation and analyzing the probability density distributions of the stochastic Model B.

Especially, we defined *RoP*, which describes the ratio of probabilities around E_0 to E_3, in order to reveal the underlying stability transition for the stochastic system. Moreover, from the perspective of two key parameters in the disturbed model, we proved the following results: firstly, noise induces the stability transition in the disturbed system from bistability to monostability. Further, there are two different monostabilities for the system, one is E_0 and the other is E_3. Secondly, noise shrinks the parametric zone of both parameters where the system remains bistable. Especially when noise is strong enough, the parametric zone of the bistable system becomes quite small. Thirdly, noise helps the system to escape from being extinct, which means that the corresponding populations are supposed to have a higher probability to persist. Therefore, noise not only causes stability transition in the system from bistability to monostability but also helps populations to avoid extinction to a large extent. In the biological systems, the extinction of avian population due to influenza is rarely observed. Our models reveal that the avian population tends to persistence under noise, which describes the reality well.

Our results were obtained with an avian epidemic model and the same analytical method could be used to study the population dynamics of various population models or transmission dynamics of other epidemic models. Moreover, it is also worth exploring the effects of noise on those models when limit cycles exist, such as the predator-prey model with Holling type II functional response [28, 29] and the Leslie-Gower predator-prey model [30].

Declaration of Competing Interest

All authors declare no conflicts of interest in this paper in this section.

CRediT authorship contribution statement

Yu Liu: Validation, Methodology, Formal analysis, Investigation, Writing - original draft, Writing - review & editing. **Shigui Ruan:** Methodology, Formal analysis, Investigation, Resources, Writing - original draft, Writing - review & editing. **Ling Yang:** Conceptualization, Methodology, Writing - original draft.

Acknowledgements

This work was partially supported by the National Key Research and Development Program of China (2018YFA0801103) and the National Natural Science Foundation of China (no. 11671417). The authors would like to thank the three anonymous reviewers for their careful comments and valuable suggestions.

Supplementary materials

Supplementary material associated with this article can be found, in the online version, at doi:10.1016/j.cnsns.2020.105416.

References

[1] Chesson P. Species Competition and Predation. In: Leemans R, editor. Ecological Systems: Selected Entries from the Encyclopedia of Sustainability Science and Technology. New York: Springer; 2013. p. 223–56.
[2] Murray JD. Mathematical Biology II: Spatial Models and biomedical applications. New York: Springer; 2003.
[3] Anderson RM, May RM. Infectious Diseases of Humans: Dynamics and Control. Oxford: Oxford University Press; 1992.
[4] Keeling MJ, Rohani P. Modeling Infectious Diseases in Humans and Animals. Princeton: Princeton University Press; 2008.
[5] Kramer AM, Dennis B, Liebhold AM, Drake JM. The evidence for Allee effects. Popul. Ecol 2009;51:341–54.
[6] Dennis B. Allee effects: population growth, critical density, and the chance of extinction. Nat. Resour. Model 1989;3:481–538.
[7] Stephens P, Sutherland W, Freckleton R. What is the Allee effect? Oikos 1999;87:185–90.
[8] Berec L, Angulo E, Courchamp F. Multiple Allee effects and population management. Trends Ecol. Evol. 2007;22:185–91.
[9] Aguirre P, González-Olivares E, Sáez E. Two limit cycles in a Leslie-Gower predator-prey model with additive Allee effect. Nonlinear Anal. Real World Appl 2009;10:1401–16.
[10] Aguirre P, González-Olivares E, Sáez E. Three Limit Cycles in a Leslie–Gower Predator-Prey Model with Additive Allee Effect. Nonlinear Anal. Real World Appl 2009;69:1401–16.
[11] Hilker F, Langlais M, Malchow H. The Allee effect and infectious diseases: extinction, multistability, and the disappearance of oscillations. Am. Nat 2009;173:72–88.
[12] Friedman A, Yakubu A-A. Fatal disease and demographic Allee effect: population persistence and extinction. J. Biol. Dynam. 2012;6:495–508.
[13] Mao X, Marion G, Renshaw E. Environmental Brownian noise suppresses explosions in population dynamics. Stoch. Proc. Appl 2002;97:95–110.
[14] Kang Y, Castillo-Chávez C. Dynamics of SI models with both horizontal and vertical transmissions as well as Allee effects. Math. Biosci 2013;248:97–116.
[15] Ji C, Jiang D, Yang Q, Shi N. Dynamics of a multigroup SIR epidemic model with stochastic perturbation. Automatica 2012;48:121–31.
[16] Yang Q, Jiang D, Shi N, Ji C. The ergodicity and extinction of stochastically perturbed SIR and SEIR epidemic models with saturated incidence. J. Math. Anal. Appl. 2012;388:248–71.
[17] Imhof L, Walcher S. Exclusion and Persistence in deterministic and stochastic chemostat models. J. Differ. Equations 2005;217:26–53.
[18] Ackleh A, Allen L, Carter J. Establishing a beachhead: a stochastic population model with an Allee effect applied to species invasion. Theor. Pop. Biol 2007;71:290–300.
[19] Ghanbari B, Gómez-Aguilar JF. Analysis of two avian influenza epidemic models involving fractal-fractional derivatives with power and Mittag-Leffler memories. Chaos 2019;29:123113.
[20] Zhang X, Shi Z, Wang Y. Dynamics of a stochastic avian-human influenza epidemic model with mutation. Physica A 2019;534:121940.
[21] Krstic M, Jovanovic M. On stochastic population model with the Allee effect. Math. Comput. Model 2010;52:370–9.
[22] Jovanović M, Krstic M. The influence of time-dependent delay on behavior of stochastic population model with the Allee effect. Appl. Math. Model 2014;39.
[23] Bashkirtseva I, Ryashko L, Spagnolo B. Combined impacts of the Allee effect, delay and stochasticity: persistence analysis. Commun. Nonlinear Sci 2020;84:105148.
[24] Liu S, Ruan S, Zhang X. Nonlinear dynamics of avian influenza epidemic models. Math. Biosci 2016;283.
[25] Higham DJ. An Algorithmic Introduction to Numerical Simulations of Stochastic Differentila Equations. SIAM Rev 2001;43:525–46.
[26] Wang J, Li C, Wang E. Potential and flux landscapes quantify the stability and robustness of budding yeast cell cycle network. P. Natl. Acad. Sci. USA 2010;107:8195–200.
[27] VCell-Modeling and Analysis Software, https://vcell.org/.
[28] Upadhyay R. Chaotic dynamics in a three species aquatic population model with Holling type II functional response. Nonlinear Anal.-Model. 2008;1.
[29] Kot M. Elements of Mathematical Ecology. Cambridge: Cambridge University Press; 2002.
[30] Guo L, Song Z-G, Xu J. Complex dynamics in the Leslie–Gower type of the food chain system with multiple delays. Commun. Nonlinear Sci 2014;19:2850–65.

Supplemental Information

Supplemental A

In this section, we give a brief introduction of the Euler-Maruyama method which was applied as our simulation method for Model B.

An autonomous SDE can often be written as:

$$dX(t) = f(X(t))dt + g(X(t))dW(t),\ X(0) = X_0,\ 0 \le t \le T, \qquad (3)$$

where $X(t)$ is a random variable for each t, f and g are scalar functions. Besides, $W(t)$ is a Brownian motion that depends continuously on $t \in [0,T]$. If $g \equiv 0$ and X_0 is constant, then the above equation reduces to the ordinary differential equation

$$dX(t)/dt = f(X(t)),\ X(0) = X_0.$$

In order to apply a numerical method to (3) over time interval $[0,T]$, the interval is discretized by $\Delta t = T/L$ for some positive integer L and $\tau_j = j\Delta t$. Also the numerical approximation to $X(\tau_j)$ will be denoted as X_j. Then the Euler-Maruyama (EM) method takes the following form:

$$X_j = X_{j-1} + f(X_{j-1})\Delta t + g(X_{j-1})(W(\tau_j) - W(\tau_{j-1})),\ j = 1,2,...,L. \qquad (4)$$

The step size Δt for the numerical method is always chosen to be an integer multiple $R \geq 1$ of the increment δt for the Brownian path. This ensures that the set of points $\{t_j\}$ on which the discretized Brownian path is based contains the points $\{\tau_j\}$ at which the EM solution is computed. As a result, the increment $W(\tau_j) - W(\tau_{j-1})$ can be generalized as:

$$W(\tau_j) - W(\tau_{j-1}) = W(jR\delta t) - W((j-1)R\delta t) = \sum_{k=jR-R+1}^{jR} dW_k, \quad k = 1, 2, ..., L,$$

where dW_k is an independent Brownian motion of the form $\sqrt{\Delta t} N(0,1)$.

Supplemental B

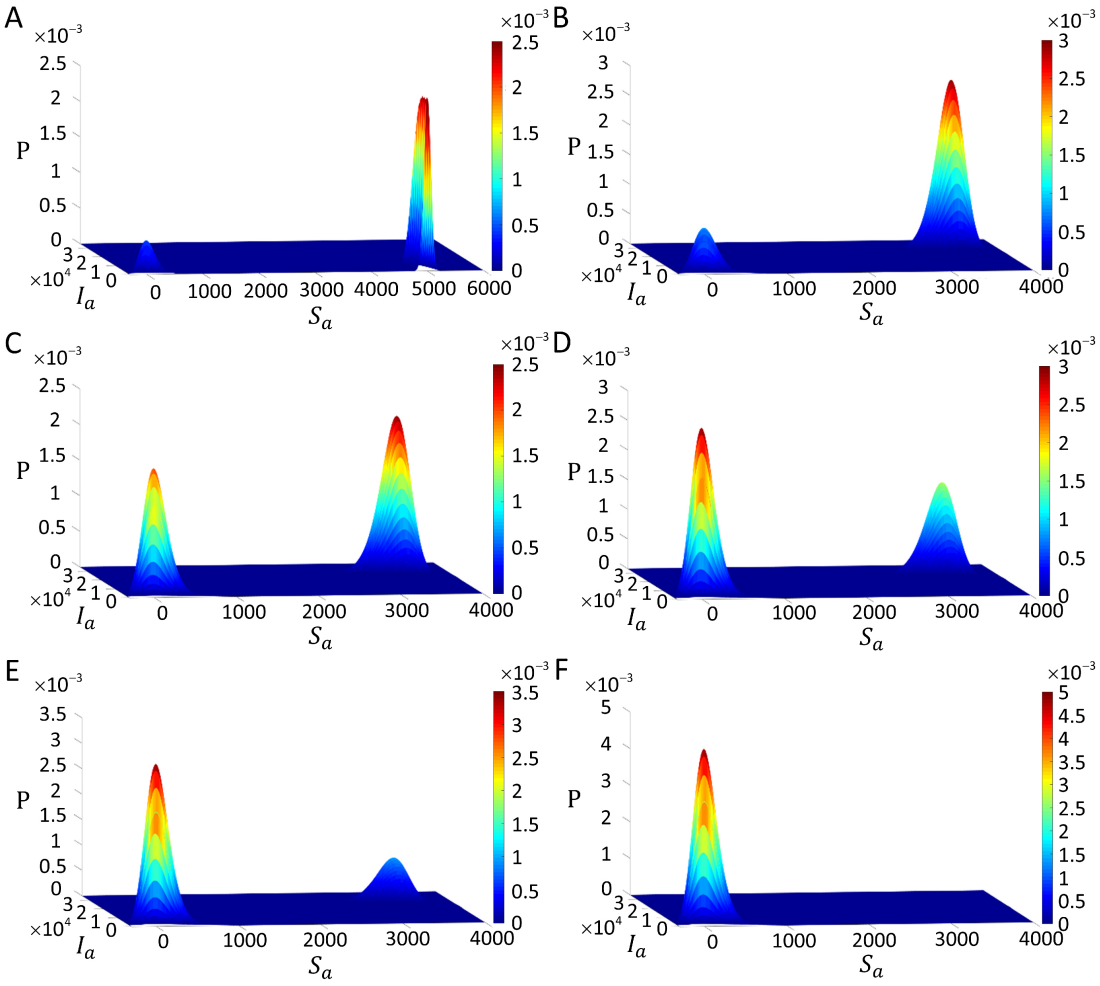

Figure S1. Probability densities for different values of β_a. $(A)\ \beta_a = 1.6\times10^{-7}$; $(B)\ \beta_a = 2.2\times10^{-7}$;

$(C)\ \beta_a = 2.24\times10^{-7}$; $(D)\ \beta_a = 2.3\times10^{-7}$; $(E)\ \beta_a = 2.36\times10^{-7}$; $(F)\ \beta_a = 2.5\times10^{-7}$.

Supplemental C

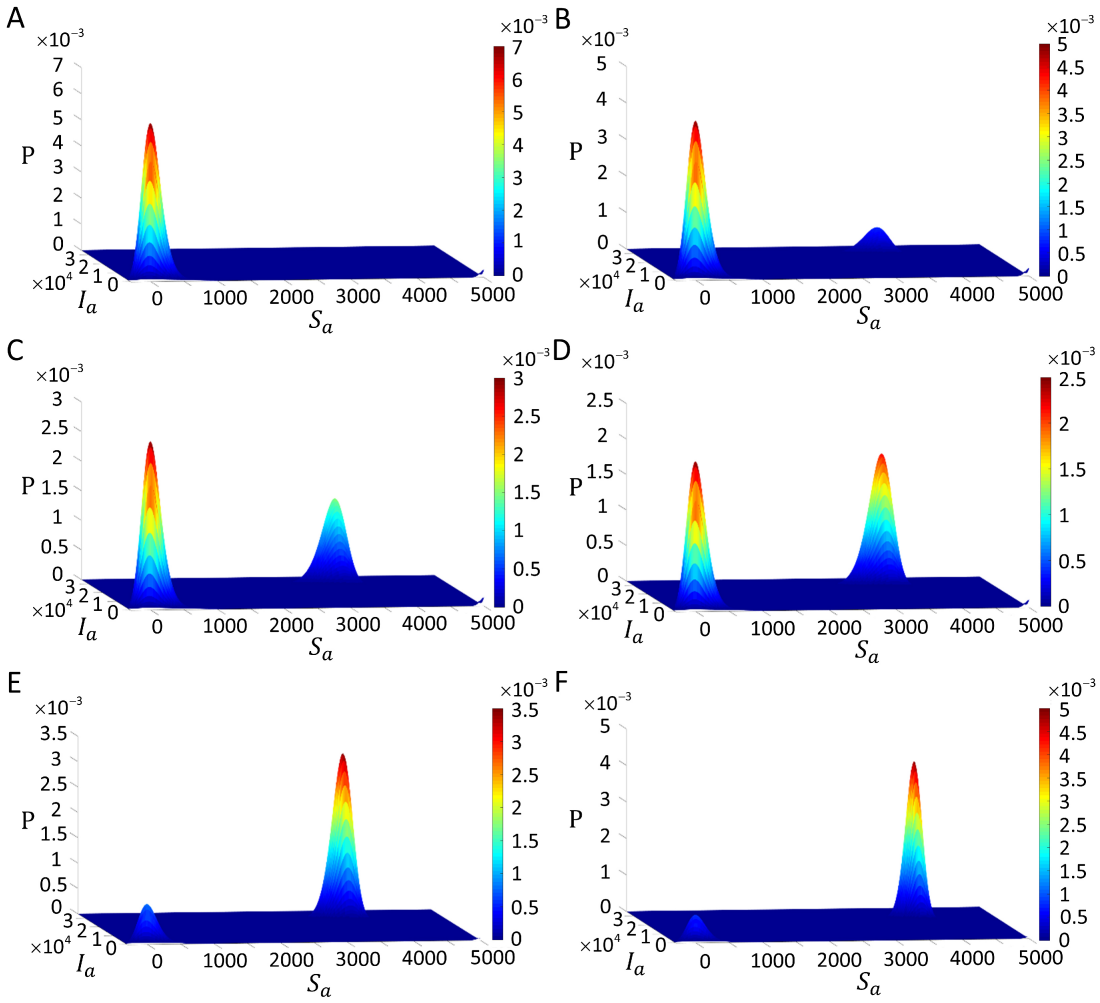

Figure S2. Probability densities for different values of μ_a. $(A)\ \mu_a = 2\times10^{-4}$; $(B)\ \mu_a = 2.45\times10^{-4}$;

$(C)\ \mu_a = 2.55\times10^{-4}$; $(D)\ \mu_a = 2.7\times10^{-4}$; $(E)\ \mu_a = 3.5\times10^{-4}$; $(F)\ \mu_a = 5.3\times10^{-4}$.